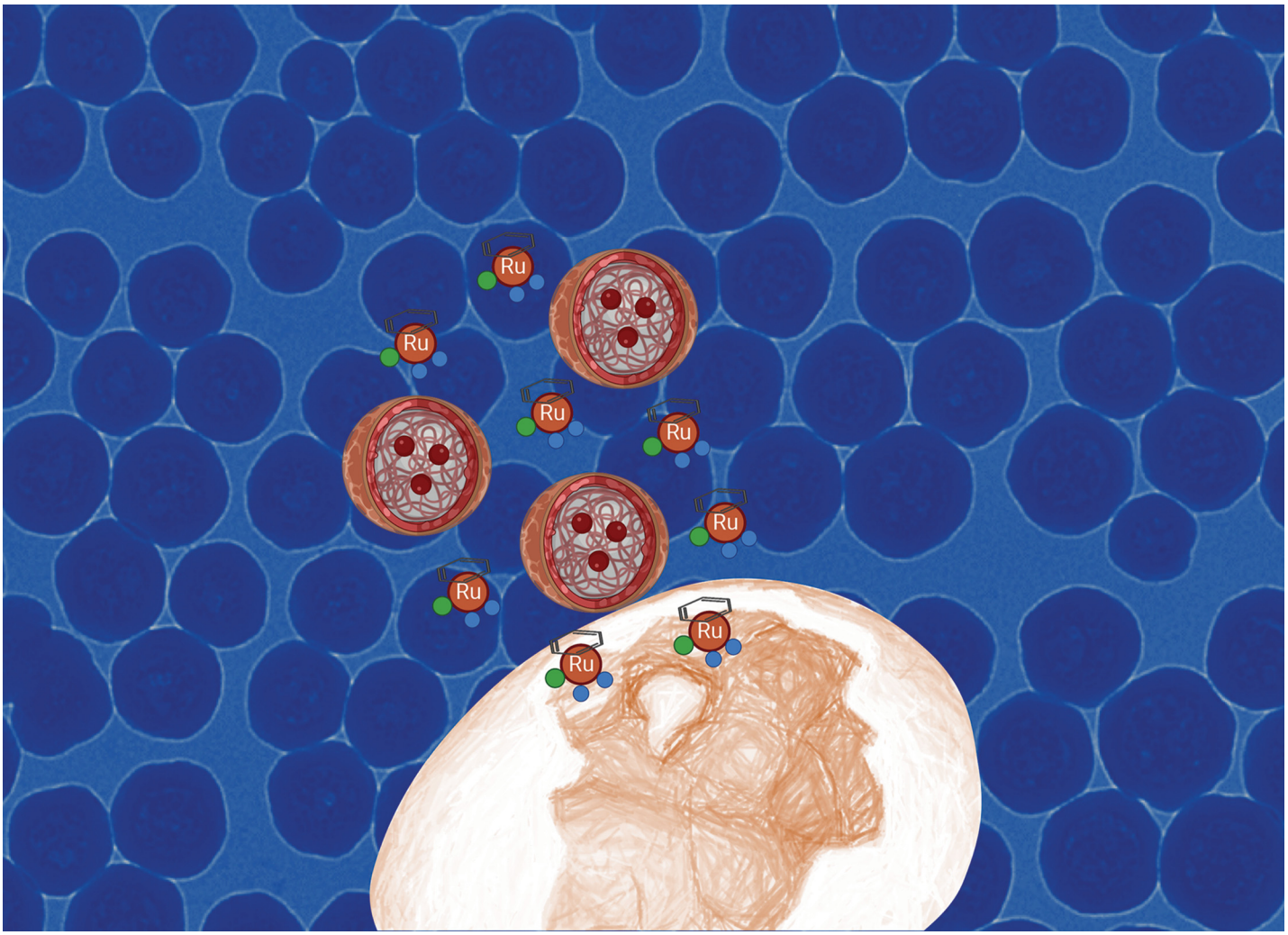

Highlighting the work from the Unit coordinated by Professor Valerio Voliani at the Center for Nanotechnology Innovation (Istituto Italiano di Tecnologia) and University of Genoa in collaboration with the University of Pisa.

Hybrid nano-architectures loaded with metal complexes for the co-chemotherapy of head and neck carcinomas

This article sheds light on the combined action of Pt and Ru metal complexes administered as free molecules or loaded into hybrid nano-architectures on head and neck carcinoma models of increasing complexity.

As featured in:

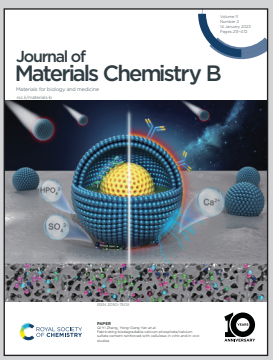

See Valerio Voliani *et al.*, *J. Mater. Chem. B*, 2023, **11**, 325.

ROYAL SOCIETY OF CHEMISTRY

rsc.li/materials-b

Registered charity number: 207890

Journal of Materials Chemistry B

ROYAL SOCIETY OF CHEMISTRY

PAPER

View Article Online
View Journal | View Issue

Cite this: J. Mater. Chem. B, 2023, 11, 325

Hybrid nano-architectures loaded with metal complexes for the co-chemotherapy of head and neck carcinomas†

Melissa Santi,‡[a] Valentina Frusca,‡[b] Maria Laura Ermini,[b] Ana Katrina Mapanao,§[b] Patrizia Sarogni,[b] Alessandra Gonnelli,[bc] Noemi Giannini,[bc] Agata Zamborlin,[bd] Lorenzo Biancalana,[e] Fabio Marchetti[e] and Valerio Voliani *[bf]

Head and neck squamous cell carcinomas (HNSCCs) are a complex group of malignancies that affect different body sites pertaining to the oral cavity, pharynx and larynx. Current chemotherapy relies on platinum complexes, the major exponent being cisplatin, which exert severe side effects that can negatively affect prognosis. For this reason, other metal complexes with less severe side effects are being investigated as alternatives or adjuvants to platinum complexes. In this context, exploiting (supra)additive effects by the concurrent administration of cisplatin and emerging metal complexes is a promising research strategy that may lead to effective cancer management with reduced adverse reactions. Here, the combined action of cisplatin and a ruthenium(II) η^6-arene compound (RuCy), both as free molecules and loaded into hybrid nano-architectures (NAs), has been assessed on HPV-negative HNSCC models of increasing complexity: 2D cell cultures, 3D multicellular tumor spheroids, and chorioallantoic membranes (CAMs). Two new NAs have been established to explore all the delivery combinations and compare their ability to enhance the efficacy of cisplatin in the treatment of HNSCCs. A significant supra-additive effect has been observed in both 2D and 3D models by one combination of treatments, suggesting that cisplatin is particularly effective when loaded on NAs, whereas RuCy performs better when administered as a free compound. Overall, this work paves the way for the establishment of the next co-chemotherapeutic approaches for the management of HNSCCs.

Received 9th September 2022,
Accepted 15th November 2022

DOI: 10.1039/d2tb01930b

rsc.li/materials-b

1. Introduction

Head and neck squamous cell carcinomas (HNSCCs) are a complex group of epithelial malignancies that affect different body sites, including the oral cavity, nasopharynx, oropharynx, larynx, and salivary glands.[1] HNSCCs are mainly caused by extensive consumption of tobacco and alcohol, but recently a new subset of head and neck cancers, with peculiar biological and clinical features, was discovered to be associated with human papillomavirus (HPV) infection.[2] HNSCCs are one of the most common cancers worldwide, with more than 900 000 new cases and 450 000 deaths in 2020, accounting for 6% of all cancers and just over 3% of all cancer deaths.[3]

The treatment approaches are associated with anatomical subsites, disease stages, disease characteristics, functional considerations and patient wishes. Although natural history is different for HPV-related than for tobacco-related HNSCC, intensive therapy is more difficult in elderly patients.[4] The current standards of care for HNSCC patients include surgery and radiotherapy, followed by chemotherapy.[5] When surgical resection is less feasible or would result in poor long-term functional outcomes, chemo-radiotherapy is the curative standard of care.[6] In these patients, a high-dose of cisplatin (100 mg m^{-2} of body-surface area, administered intravenously every 21 days for three cycles) concurrently with radiotherapy is the common treatment with established survival benefits for patients with good performance status. However, because of substantial short- and long-term toxic effects associated with cisplatin, its use is predominantly reserved for nonelderly patients who have no

[a] NEST Istituto Nanoscienze-CNR and Scuola Normale Superiore, 56127, Pisa, Italy
[b] Center for Nanotechnology Innovation@NEST, Istituto Italiano di Tecnologia, Piazza San Silvestro 12, 56127, Pisa, Italy
[c] Radiation Oncology Unit, Pisa University Hospital, Via Roma 67, Pisa, Italy
[d] NEST-Scuola Normale Superiore, Piazza San Silvestro 12, 56127 Pisa, Italy
[e] Department of Chemistry and Industrial Chemistry, University of Pisa, Via Moruzzi 13, 56124 Pisa, Italy
[f] Department of Pharmacy, University of Genoa, Viale Cembrano, 4-16148, Genoa, Italy. E-mail: valerio.voliani@unige.it

† Electronic supplementary information (ESI) available. See DOI: https://doi.org/10.1039/d2tb01930b

‡ Equal contribution.

§ Current address: Center for Radiopharmaceutical Sciences, Paul Scherrer Institute, 5232 Villigen-PSI, Switzerland.

major coexisting conditions. For patients with lower levels of fitness and patients in whom high-dose cisplatin is associated with unacceptable adverse effects, alternative systemic therapies are under investigation.[6]

The combination of chemotherapeutic agents may result in an improved efficacy in the treatment of malignancies compared to the effects of a single agent. The additive or synergistic effects of multiple agents usually lead to noticeably higher clinical benefits.[7] In this scenario, adjuvant drugs are increasingly demanded to reduce the adverse reactions associated with the cisplatin chemotherapy doses.

Recently, the chemistry of ruthenium complexes has received increasing interest due to the potential anticancer behavior of many derivatives. Some ruthenium-based anticancer metallotherapeutics have demonstrated activity against some cisplatin-resistant cell lines with less severe side effects compared to cisplatin and its derivatives.[8] To date, only a handful of ruthenium(III) therapeutics has entered clinical trials[9,10] but have not yet initiated or completed a phase II study.[11] Since the mode of action of these compounds is supposed to involve ruthenium(III) to ruthenium(II) reduction in the tumor environment, Ru(II) complexes have been intensively investigated and [$RuCl_2$(PTA)(η^6-*p*-cymene)], comprising the amphiphilic phosphine 1,3,5-triaza-7-phosphatricyclo[3.3.1.1]decane (PTA) and known as RAPTA-C, emerged as a promising compound (Fig. S1A, ESI†).[12] RAPTA-C acts on the angiogenesis processes of tumors (not on necrosis/apoptosis), reducing the formation of new vessels and limiting the access of malignant cells to oxygen and nutrients.[13,14] Recently, we developed new robust ruthenium(II) arene complexes and their activity was tested in 3D models of ± HPV HNSCC cell lines.[15] These series of compounds are formed by cationic ruthenium(II) *p*-cymene complexes bearing α-diimine ligands, of general formula [RuCl{κ^2*N*-(HC = NR)$_2$}(η^6-*p*-cymene)]NO_3, which show high stability in biological media and good solubility in water.[16,17] In particular, RuCy (R = cyclohexyl, Fig. S1B, ESI†) showed good toxic activity on HNSCC cell lines with an IC_{50} < 100 μM at 72 h after treatment (2 h exposure to the drug).[15]

In general, ruthenium complexes represent interesting alternatives to cisplatin as well as potential adjuvants in co-chemotherapy approaches. Noticeably, very few studies explored the combined effect of cisplatin and other metal complexes in the treatment of neoplasms.[18]

Here, the combined effect of cisplatin and RuCy has been evaluated on models of HPV-negative HNSCCs of increasing complexity. In particular, we evaluated three different delivery approaches for the simultaneous administration of cisplatin and RuCy: (i) as free compounds, (ii) both included in a specifically designed hybrid nanoarchitecture (NA), and (iii) in a mixed strategy including free RuCy and cisplatin loaded into NAs. NAs are hybrid nano-architectures composed of biodegradable silica capsules containing a polymeric matrix and ultrasmall metal nanoparticles.[19] The extreme versatility of the synthetic protocol allows for the loading of active molecules in the inner cavity as well as for surface functionalization.[20,21] The NA family has been developed to avoid the issue of plasmon nanomaterial persistence after the action with a special focus on oncology.[22,23] Moreover, the presence of ultra-small gold nanoparticles in NAs is pivotal to further enhance their potential combined applications in photothermal therapy as well as in diagnostic photoacoustic imaging.[24,25] The combined effect of the three strategies has been assessed on 2D cell cultures, 3D multicellular tumor spheroids, and chorioallantoic membranes (CAMs) in agreement with the European Parliament Directive 2010/63/EU. CAMs are *in vivo* alternative models for the reliable evaluation of innovative approaches for cancer detection and treatment.[26] Indeed, the highly vascularized membrane of CAMs can be exploited to support the development of tumor xenografts, to study the angiogenesis-related mechanisms and/or to examine the anti-metastatic/antitumor activity of the treatments.[21,27]

Overall, our investigation shows that co-chemotherapy based on nanomaterials is a promising strategy for cancer management and that the use of alternative *in vivo* models is crucial in oncological preclinical research.

2. Materials and methods

2.1 Synthesis of gold nanoparticles

All nanoparticles were formulated starting from a standard protocol for the synthesis of NAs as described previously.[19] Briefly, ultrasmall gold nanoparticles with a diameter of approximately 3 nm were prepared by adding 20 μL of poly(sodium 4-styrene sulfonate) (PSS, 30% aqueous solution) and 200 μL of $HAuCl_4$ aqueous solution (10 mg mL^{-1}) to 20 mL of milliQ® water. During stirring, 200 μL of sodium borohydride (8 mg mL^{-1} in milliQ water) was added quickly to the mixture that was then mixed for another 2 minutes. The solution was aged for 10 minutes at room temperature and became brilliant orange.

2.2 Synthesis of drug-loaded nano-architectures (NAs)

NAs-CisPt and NAs-CisPt-RuCy gold aggregates were prepared using a modified poly(L-lysine) loaded with cisplatin prodrug, synthesized as described below.

2.2.1 Synthesis of c,t,c-[$PtCl_2(OH)_2(NH_3)_2$]. The method was based on what was previously described by Hall *et al.*[28] cis-[$PtCl_2(NH_3)_2$] powder (0.40 g, 1.33 mmol) was suspended in milliQ® water (10 mL) and H_2O_2 30% (w/v) (14 mL, ten-fold excess) was added. The mixture was mixed for 1 h at 50 °C. Then, it was cooled in an ice bath to reach 0 °C and a saturated water solution of NaCl (10 mL) was added. The resultant pale yellow powder was filtrated and washed with cold water and ethanol and dried in a vacuum pump, yielding c,t,c-[$PtCl_2(OH)_2(NH_3)_2$] (223 mg, 0.67 mmol, 50%).

2.2.2 Synthesis of c,t,c-[$PtCl_2(NH_3)_2(OH)(O_2CCH_2CH_2CO_2H)$]. We used a modified method already described elsewhere.[29] c,t,c-[$PtCl_2(OH)_2(NH_3)_2$] (0.2 g, 0.6 mmol) was suspended in anhydrous dimethyl sulfoxide (DMSO, 16 mL) and succinic anhydride (0.06 g, 0.6 mmol) was added to the solution and stirred at room temperature for 12 h. The solution was freeze-dried and acetone (10 mL) was added to precipitate a light yellow solid, which was collected by filtration and washed several times with acetone,

diethyl ether, and then dried in a vacuum pump, yielding c,t,c-[$PtCl_2(NH_3)_2(OH)(O_2CCH_2CH_2CO_2H)$] (0.16 g, 0.37 mmol, 62%).

2.2.3 Synthesis of drug-modified poly(L-lysine) (PL-CisPt). 0.5 mg of c,t,c-[$PtCl_2(NH_3)_2(OH)(O_2CCH_2CH_2CO_2H)$] powder was dissolved in 400 μL of PBS buffer and mixed with freshly made EDC/NHS (40 μL, 0.21 M) milliQ® water solution (EDC: *N*-(3-dimethylaminopropyl)-N0-ethylcarbodiimide hydrochloride, NHS: *N*-hydroxysuccinimide). The mixture was stirred for 10 minutes at room temperature and then poly(L-lysine) hydrobromide 15–30 kDa (75 μL, 20 mg mL^{-1} milliQ® solution) was added to the reaction. The resulting solution was stirred overnight at room temperature. The modified poly(L-lysine) was collected and washed three times with PBS buffer using Amicon 10 kDa filter units and then dissolved in PBS buffer (800 μL).

2.2.4 Synthesis of NAs-CisPt aggregates. NAs-CisPt aggregates were synthesized starting from a 20 mL aqueous solution of ultrasmall gold nanoparticles. 165 μL of PL-CisPt was slowly added to the solution, and then stirred for 20 minutes at room temperature. Aggregates were collected by centrifugation (13 400 rpm for 3 min) and resuspended in 2 mL of milliQ® water. The solution was sonicated for a maximum of 4 minutes to resuspend aggregates.

2.2.5 Synthesis of NAs-CisPt-RuCy aggregates. RuCy was synthesized as described in our works.[15,17] NAs-CisPt-RuCy aggregates were also synthesized starting from a 20 mL aqueous solution of ultrasmall gold nanoparticles added with 210 μL of a solution of RuCy (24 mg mL^{-1} in milliQ®:DMSO, 1:2). Upon addition of RuCy, the reaction mixture turned from brilliant orange to brown. Then, 75 μL of PL was added to the solution that was allowed to stir at room temperature for 20 minutes and then centrifuged to collect aggregates. The arrays were suspended in 2 mL of milliQ® water and sonicated for a maximum of 4 minutes.

2.2.6 Synthesis of NAs-RuCy aggregates. NAs containing no gold nanoparticles were also synthesized from a solution of 20 mL of milliQ water and 10 μL of PSS by adding first 210 μL of RuCy solution (24 mg mL^{-1} in milliQ®:DMSO, 1:2) and then adding 75 μL of PL. Arrays were collected by centrifugation and resuspended in 2 mL of milliQ® water by sonication. The appearance of the reaction mixture shifted from colorless to yellow upon the addition of RuCy.

2.2.7 Synthesis of complete nano-architectures. The last step is the formation of the silica shell around aggregates that is the same for all the types of nanoparticles. We used a modified Stöber method described as follows: 70 mL of absolute ethanol was mixed with 40 μL of tetraethyl orthosilicate (TEOS, 98%) and 2.4 mL of ammonium hydroxide solution (30% in water). Then, 2 mL of the gold nanoparticle arrays previously prepared was added to the mixture, and the solution was allowed to gently shake at room temperature for 3 h (3.5 h for NAs-RuCy and NAs-CisPt-RuCy). The synthesized nanoarchitectures were collected by 30 min centrifugation at 4000 rpm, washed twice with ethanol and suspended in 1 mL of ethanol. A short spin centrifugation was employed in order to separate the structures with diameters larger than 150 nm from the supernatant. The solution containing about 1.5 mg of NAs was stored at −20 °C until use. It remains usually stable for at least one year. All types of nanoparticles were fully characterized to verify the success of the synthetic process.

2.3 Dynamic light scattering (DLS) and zeta-potential measurements

The DLS measurements were performed at 37 °C in a 1 mL quartz cuvette on a Zetasizer nano-ZS90 (Malvern Instruments, Malvern, United Kingdom) following the manufacturer's instructions. The nanomaterials were diluted to 0.15× and suspended in PBS and analyzed with a single scattering angle of 90°. For the zeta-potential measurements, the sample was transferred into DTS 1070 standard capillary cells. The values reported are the average of four consecutive measurements.

2.4 UV-Vis spectrophotometry

UV-Vis spectra were recorded using a Mettler Toledo UV5 Nano spectrophotometer, using the micro-volume platform. The nanoparticles were dissolved in 1× PBS solution and an aliquot of 3 μL was used for the measurements.

2.5 Inductively coupled Plasma-Mass spectrometry (ICP-MS) analysis

An aliquot (10 μL) of the nanoparticles was placed in a pressure vessel and dissolved in 200 μL of aqua regia. The sealed vessel was placed in CEM Discover SP-D for further digestion under microwave irradiation (200 °C/15 min). The sample was then diluted with 3% nitric acid to 4 mL. The amounts of elemental gold, platinum or ruthenium were determined after analysis using an ICP-MS Agilent 7700 (Agilent Technologies, Santa Clara, CA, USA), using standard calibration curves. A 10 ppm of Hg solution in 3% nitric acid was used as an internal standard.

2.6 Transmission electron microscopy characterization

The TEM observations of all nanoparticles were performed using a ZEISS Libra 120 PLUS operating at 120 KV and equipped with an In-column Omega filter. The suspensions with the nanoparticles (5 μL) were deposited on a 300-mesh carbon coated copper grid and allowed to dry before image acquisition.

2.7 Release assay

An aliquot of 500 μL of NAs-RuCy was resuspended in 100 μL of HEPES buffer (20 mM, pH 7.4) and placed in a dialysis membrane (molecular weight cut-off: 10 kDa). The membrane was then placed in a 50 mL tube with 15 mL of HEPES buffer. The solution was maintained at 37 °C under stirring for 7 days. For every time point, an aliquot (3 mL) of buffer was drawn and the ruthenium content was analyzed using ICP-MS.

2.8 Cell culture

The SCC-25 cell line was purchased from the American Type Culture Collection (ATCC) and cultured following the manufacturer's instructions. Cells were maintained in a mixture of Dulbecco's modified Eagle and Ham's F12 (DMEM/F12 1:1) from Invitrogen (Carlsbad, CA, USA). The medium was also

supplemented with 10% fetal bovine serum (FBS), 4 mM L-glutamine, 1 mM sodium pyruvate, 100 U mL^{-1} penicillin, 100 mg mL^{-1} streptomycin (Invitrogen) and 400 ng mL^{-1} hydrocortisone (Merck). The cells were maintained at 37 °C in a humidified 5% CO_2 atmosphere. For 3D models, we used a protocol previously described by us.[30] Briefly, the cells were harvested and centrifuged for 5 min at 1200 rpm. Then, the cells were suspended in fresh medium and counted and the suspension was adjusted to a final concentration of 1×10^6 cells mL^{-1}. Then, 10 μL drops of cell suspension were placed on the lid of a 100 mm cell culture dish that was flipped into the chamber containing 10 mL of PBS to avoid dehydration of the drops. The drops were maintained in an incubator at 37 °C until the cells formed a sheet and then were transferred to a 100 mm suspension culture dish after 3 days. Finally, cell aggregates were placed inside a CO_2 incubator with an orbital shaker (60–70 rpm) for 24 h to induce the formation of the final spherical conformation.

2.9 Viability assays

The viability on 2D cell cultures was evaluated for the SCC-25 cell line after treatment with different combinations of NAs and ruthenium arene complexes. In all cases, 10^4 cells/well were seeded in 96 well plates and grown for 24 h at 37 °C and 5% CO_2. Then, the cells were treated for 2 h at 37 °C and washed twice with PBS, and the viability was measured at 24, 48 and 72 h after treatments. Cytotoxicity was evaluated using a tetrazolium salt, 2-(2-methoxy-4-nitrophenyl)-3-(4-nitrophenyl)-5-(2,4-disulfophenyl)-2H tetrazolium, and monosodium salt (WST-8) assay (Tebu-Bio). For each experimental time point, cells were incubated with WST-8 reagent (10 μL) and medium (90 μL) for 2 h. Absorbance (450 nm) was measured using a microplate reader (Glomax Discovery, Promega, Madison, WI, USA). The percentage of cell viability was determined by comparing drug-treated cells with the untreated cells (100% viability). Viability of 3D spheroids was evaluated using a CellTiter-Glo® 3D Cell Viability Assay (Promega, Milan, Italy). Spheroids for each time point were transferred from a round-bottom 96 well plate to a white 96 well plate (one spheroid for one well in 100 μL of medium) for luminescence measurements. Then, 100 μL of CellTiter-Glo® 3D reagent was added to each well, the plate was shaken for 5 min, and the luminescence signal was recorded after 25 min of incubation using a microplate reader (Glomax Discovery, Promega, Madison, WI, USA). Cell viability was determined with respect to the viability of spheroids maintained in a complete medium without treatments. Data represent the average of three independent experiments, and the error bars represent the standard deviation.

2.10 CAM assay

Red Leghorn chicken eggs were incubated at 37 °C in a fan-assisted humidified egg incubator (FIEM). For detailed procedures, please refer to the methods already published by our group.[27] Briefly, from Embryonic Day of Development 0 (EDD0) to EDD3, the eggs were positioned horizontally and rotated to allow the natural formation of the air chamber. On EDD3, a small hole was created on the blunt end of each egg with tweezers. The eggs were then positioned vertically, and at EDD6, a small window of about 1 cm^2 was created to allow the grafting of 2×10^6 SCC-25 cells in a cell culture medium and Matrigel (Corning, Ref. 354234) with a ratio of 1 : 1. At EDD10, the tumor-bearing embryos were randomized and divided into different groups of treatment. 10 μg of RuCy complex was calculated for the treatment. The right amount of powder was dissolved in the DMSO solution keeping the volume as low as possible to maintain a final % v/v of DMSO lower than 5% (this percentage is harmless for eggs, data not shown). An aliquot of NAs-CisPt was taken such that each tumor would also be treated with 4 μg of Pt per egg. Tumors were treated topically with RuCy alone, NAs-CisPt alone and RuCy and NAs-CisPt combined. All materials were administered topically after resuspension in 30 μL of serum-free medium. The embryo viability and the tumor size were monitored every two days, and the tumor volume was calculated using a modified ellipsoid formula: volume = 1/2 (length × width^2).[31] At EDD14, the chicken embryo movements were slowed down by hypothermia (2 h at 4 °C) and then the tumors were harvested. After 24 h at 4 °C, the organs (heart, liver, lungs) were collected from the embryos. The samples (tumors, organs) for ICP-MS were stored at −80 °C until analysis. All the *in vivo* experiments were performed in compliance with the current European and Italian laws and do not require approval.[26]

2.11 Conductivity and NMR studies on RuCy

General details. A D_2O solution containing dimethyl sulfone (Me_2SO_2; $c = 6.1 \times 10^{-3}$ M) as an internal standard was used in the following experiments. NMR spectra were recorded on a JEOL YH JNM-ECZ400S instrument equipped with a Royal HFX Broadband probe. ^{1}H NMR chemical shifts are referenced to the Me_2SO_2 signal as in pure D_2O or DMSO-d_6 (δ/ppm = 3.14 and 3.10, respectively). ^{35}Cl NMR chemical shifts are referenced to 1 M NaCl in D_2O (external standard). Conductivity measurements were carried out using an XS COND 8 instrument (cell constant = 1.0 cm^{-1}) equipped with NT 55 temperature probe (measurements automatically adjusted to 25 °C). Conductivity and NMR data are reported in the Supplementary Information (Tables S2 and S3, ESI†). The residual amount of RuCy in solution (% with respect to the initial spectrum) was calculated by the relative integral with respect to Me_2SO_2.

Experimental procedures. (i) NMR. RuCy (*ca.* 5 mg) was dissolved in D_2O containing 1% v/v DMSO or in a D_2O/DMSO-d_6 1 : 2 v/v mixture (0.75 mL). The yellow solutions (tot 0.75 mL; $c_{Ru} \approx 1 \times 10^{-2}$ M) were filtered over Celite, transferred into an NMR tube and maintained at room temperature (22 °C). ^{1}H (delay time = 4 s, number of scans = 20) and ^{35}Cl NMR analyses were performed after 0, 6 and 24 h.

(ii) Conductivity. RuCy (*ca.* 5 mg) was dissolved in ultrapure H_2O containing 1% v/v DMSO or in a H_2O/DMSO 1 : 2 v/v mixture. The yellow solutions (20 mL; $c_{Ru} = 4.9 \times 10^{-4}$ M) were maintained at room temperature (22 °C) and the conductivity was measured after 0, 1, 3, 5, 24 and 48 h. The conductivity of [Bu_4N]Br solutions (1.9×10^{-3} M) in 1% v/v DMSO or in an H_2O/DMSO 1 : 2 v/v was measured as a reference 1 : 1 electrolyte.

3. Results and discussion

3.1 Synthesis and characterization of NAs-CisPt, NAs-RuCy and NAs-CisPt-RuCy

The nano-architectures have been synthesized by employing standard protocols with some modifications due to the encapsulation of the ruthenium complex (NAs-RuCy) and of both the metallic drugs (NAs-CisPt-RuCy).[19] A schematic explanation of the steps involved in the synthesis is reported in Fig. 1A. In general, a colloidal solution of ultrasmall gold nanoparticles (USNPs) is prepared in the presence of poly(sodium-4-styrene sulfonate) (PSS). Then, the USNPs are aggregated with poly-L-lysine (PL) in presence of the drugs, and the USNP arrays are employed as templates for the composition of the silica nano capsules. The standard characterization data for NAs-CisPt-RuCy, NAs-CisPt, and NAs-RuCy are reported in Fig. 1 and Fig. S2 and S3 (ESI†), respectively. The measured TEM diameters and zeta-potentials for each type of NAs are reported in Table 1. It is worth noticing that cisplatin is loaded into nanoparticles as a prodrug with the metal center in the form Pt(IV). A Pt(IV) complex has been preferred to Pt(II) compounds due to the reduced off-target toxicity, decreased drug inactivation and longer half-life in the bloodstream. The prodrug is covalently linked to poly-L-lysine, and it is efficiently released inside cells by thiol activation (*e.g.*, glutathione, GSH). RuCy is included into NAs as an adsorbed compound.

Table 1 Physical-chemical characterization of the nano-architectures

	Diameter in PBS (nm-DLS)	Diameter (nm-TEM)	Zeta-potential (mV)
NAs-CisPt	227 ± 1	150 ± 26	−20 ± 1
NAs-RuCy	195 ± 9	138 ± 22	−19.3 ± 1.3
NAs-CisPt-RuCy	214 ± 19	138 ± 13	−21.0 ± 1.3

The ruthenium complex in NAs-RuCy is loaded with a non-covalent strategy (as opposed to cisplatin in NAs-cisPt); thus, the release of the ruthenium compound from NAs-RuCy has been investigated. NAs-RuCy has been incubated in HEPES buffer at 37 °C for 7 days, and for each time point, an aliquot of buffer was drawn and analyzed by ICP-MS to measure the

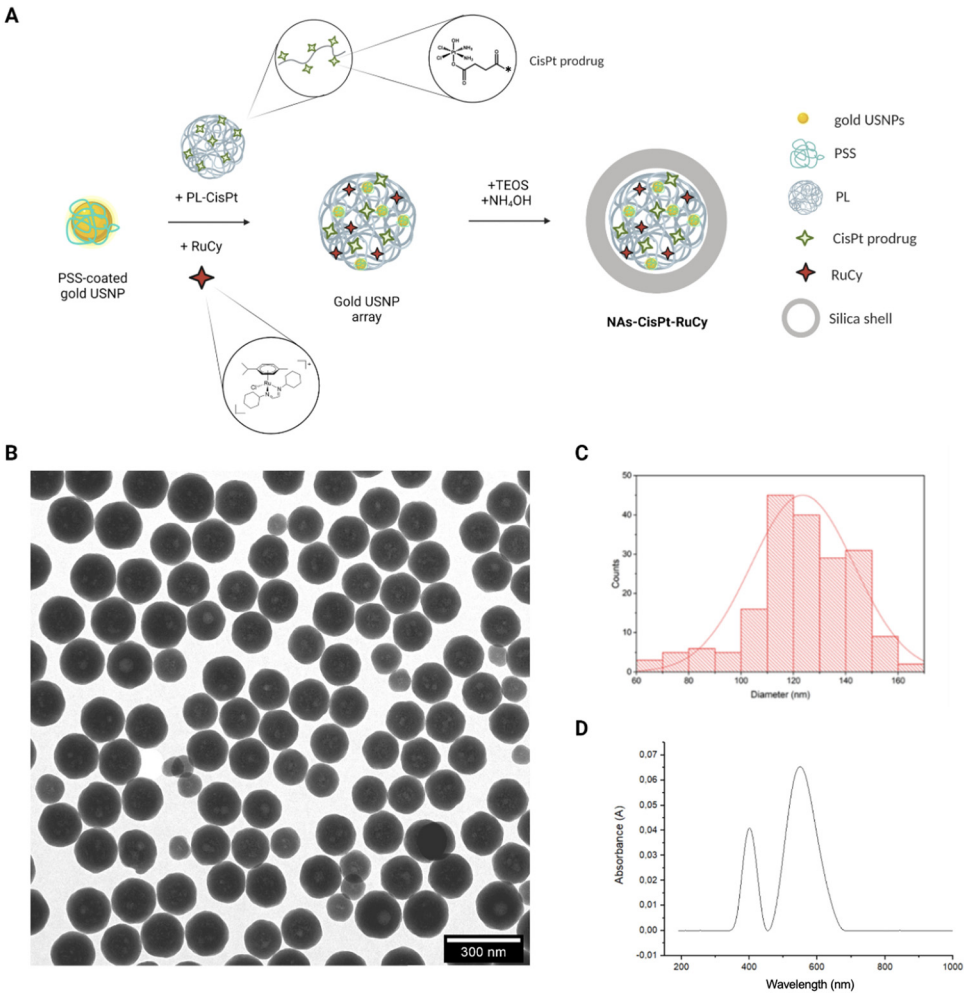

Fig. 1 (A) Schematic representation of the synthetic process for NAs-CisPt-RuCy. (B) TEM images of NAs-CisPt-RuCy. Scale bar: 300 nm. (C) Size histogram of NAs-CisPt-RuCy made on at least 100 NAs observed with TEM. The diameter of NAs was analyzed with ImageJ. (D) Background subtracted UV-Vis spectrum of NAs-CisPt-RuCy.

ruthenium content. The release profile suggested an exponential release in the first 100 h followed by a plateau (Fig. S4A, ESI†), in agreement with the partial degradation of the silica capsules (Fig. S4B, ESI†) in buffers.[18]

3.2 2D viability assay

The cells have been treated with a fixed concentration of cisplatin (IC_{50}^{CisPt} on SCC-25 : 10 μM),[32] and increasing concentrations of RuCy from 50 to 200 μM (IC_{50}^{RuCy} on SCC-25 : 80 μM) for 2 h.[15] Different RuCy concentrations were assessed in order to observe a potential combined effect of the two drugs on cell viability. To determine the combined effect, the synergistic coefficient (α) has been calculated for combined CisPt/RuCy treatment compared to CisPt and RuCy alone by using:

$$\alpha = (SF^{a} \times SF^{b})/SF^{ab}$$

where SF is the survival fraction, *a* is the CisPt treatment alone, *b* is the RuCy treatment alone and *ab* is the resulting combination. If $\alpha < 1$, the effects are antagonistic, if $\alpha = 1$, the effects are additive or null and if $\alpha > 1$, the effects are synergistic.[33] A synergistic effect was observed from 48 h after the co-chemo treatment (Fig. S5, ESI†) and confirmed by the α values (Table S1, ESI†). The statistical analysis showed that a significant difference in the samples treated with the free drugs is observed only with RuCy 200 μM. However, by the combination with NAs-CisPt + RuCy, a statistically significant difference has been also observed at a RuCy concentration of 100 μM.

In order to investigate a potential enhanced effect of the co-treatment associated with the inclusion of the drugs in a single nanoplatform, NAs-CisPt-RuCy was tested and compared on the same cell line (Fig. S6A, ESI†). Indeed, the inclusion of drugs in nanoparticles should promote their internalization by increasing their local concentration within the cells which usually results in an improved cytotoxic effect.[34] NAs-CisPt-RuCy contains cisplatin prodrug and RuCy at a concentration of 40 μM and 400 μM, respectively. The 1 : 10 ratio well matches the IC_{50} ratio calculated for the single drugs used for the investigations regarding the molecular drugs. Surprisingly, NAs-CisPt-RuCy did not show cytotoxic effects on 2D SCC-25 cells (Fig. S6A, ESI†) except for a small decrease in viability at very high concentrations. This result can be ascribed to a possible irreversible interaction between the components of NAs, which prevents both drugs from exerting their cytotoxic effects on cells. In order to shed light on the potential interactions between RuCy and gold USNPs, NAs-RuCy (NAs loaded with RuCy and without gold USNPs) were tested on SCC-25. The viability data (Fig. S6B, ESI†) confirmed that NAs-RuCy had no cytotoxic effect on cells. In this respect, RuCy demonstrated remarkable stability in water with 1% DMSO or water/DMSO 1 : 2 v/v (*i.e.* the dilute and stock solutions, respectively, employed in the formation of NAs-RuCy) at room temperature (Table S2, ESI;† 95–98% residual starting material by ^{1}H NMR after 24 h). Nevertheless, a slow solvolytic process occurs in these conditions, manifested by the release of chloride (^{35}Cl NMR) and the increase in molar conductivity (Table S3, ESI†). We hypothesize that the resulting dicationic solvato complex might interact with the polymeric matrix, for instance with the amine groups in the PL backbone. Since ruthenium is released from NAs-RuCy in buffer (Fig. S4, ESI†), such interaction may be responsible for the degradation of RuCy that might impair its functionality or for the steady maintenance of an amount of RuCy in the cytosol that may stimulate the cellular metabolism. In order to exploit the features of both drugs for co-chemotherapy, another strategy has been investigated by applying NAs loaded with cisplatin (NAs-CisPt) in combination with molecular RuCy (Fig. 2A). As expected, this approach resulted in a significant synergism (Table 2) from 24 h after treatment with both RuCy

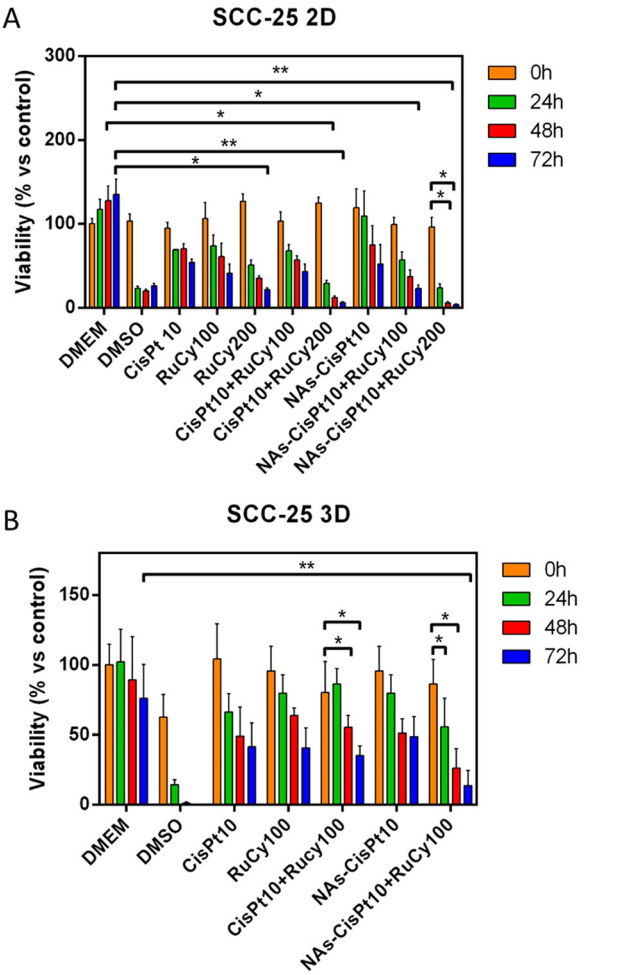

Fig. 2 Viability assays on SCC-25. (A) Treatment of 2D cell cultures with NAs-CisPt at a fixed concentration (10 μM in cisplatin prodrug) and two concentrations of RuCy co-administered as a free drug (100 μM and 200 μM). The cells were incubated with nanoparticles for 2 h, then washed twice with PBS, and the viability was measured after 24, 48 and 72 h. The viability measurements are normalized by the control (untreated cells - DMEM). Two-way ANOVA with Turkey's multiple comparison test, $*p \leq 0{,}05$ and $**p \leq 0.003$. (B) Treatment of 3D cell cultures with a fixed concentration of CisPt and RuCy (10 μM and 100 μM respectively) administered with different formulations. Spheroids were treated for 2 h and then washed twice with PBS. The viability was measured compared to the control represented by cells not treated (DMEM). Two-way ANOVA with Turkey's multiple comparison test, $*p \leq 0{,}05$ and $**p \leq 0.003$. All results are obtained from 3 independent experiments and error bars show the standard deviation.

Table 2 Synergistic coefficient (α) calculated for a combined effect of NAs-CisPt and RuCy with respect to treatments alone on 2D and 3D cell cultures

	α Coefficient		
Treatment	24 h	48 h	72 h
2D Cell cultures			
NAs-CisPt10 + RuCy100	1.1	1.1	0.9
NAs-CisPt10 + RuCy200	1.9	3.8	2.4
3D Spheroids			
CisPt10 + RuCy100	0.6	0.6	0.5
NAs-CisPt10 + RuCy100	1.1	1.2	1.4

concentrations (100 μM and 200 μM), confirming that the combined treatment is particularly effective when cisplatin is loaded in NAs and RuCy is administered as a free compound.

3.3 3D viability assay

In order to validate the data obtained on 2D cellular cultures, a more complex bio-model has been employed to evaluate the most promising co-chemo treatment approach. In this regard, multi-cellular tumor spheroids (MCTSs) represent an excellent platform for the progress of preclinical oncological investigations and the translation of nanomaterials to the clinics.[35] Indeed, MCTSs can mimic some features and complexities of both the tumor and the extracellular environment and are widely used for drug screening in agreement with the 3Rs concept to reduce and optimize the use of animals.[36,37] The 3D spheroids of SCC-25 have been produced by a standardized protocol.[30] Considering the findings on 2D cell cultures and the next *in vivo* evaluations, the spheroids have been treated with fixed concentrations of the drugs, corresponding to the lowest effective dose in 2D (10 μM for CisPt and 100 μM of RuCy). MCTSs have been treated with the drugs for 2 h and then washed twice with PBS before measuring the viability. Significative differences in the viability of spheroids treated with the combination of the drugs have been observed (Fig. 2B). Noticeably, a synergistic effect was appreciable only for the approach that employed NAs-CisPt, while the use of free drugs results in an antagonistic effect (Table 2).

3.4 CAM assay

The best combination of the treatments (NAs-CisPt + RuCy) has been finally evaluated by employing the chorioallantoic membrane (CAM) models, an optimized *in vivo* system that supports the formation of solid and vascularized tumors. The direct monitoring of tumor growth on the CAM allows the reliable evaluation of the tumor-shrinking effects due to the therapeutic treatment applied as well as the cancer behaviors associated with the treatment response.[21] In this study, the potential antitumor effect of RuCy has been assessed as a single or combined treatment with NAs-CisPt. Hence, at Embryonic Day of Development (EDD) 10, the tumor-bearing embryos have been randomized and divided into four groups: (I) serum-free cell culture medium (control), (II) RuCy, (III) NAs-CisPt and (IV) NAs-CisPt + RuCy. Tumors were topically treated and monitored

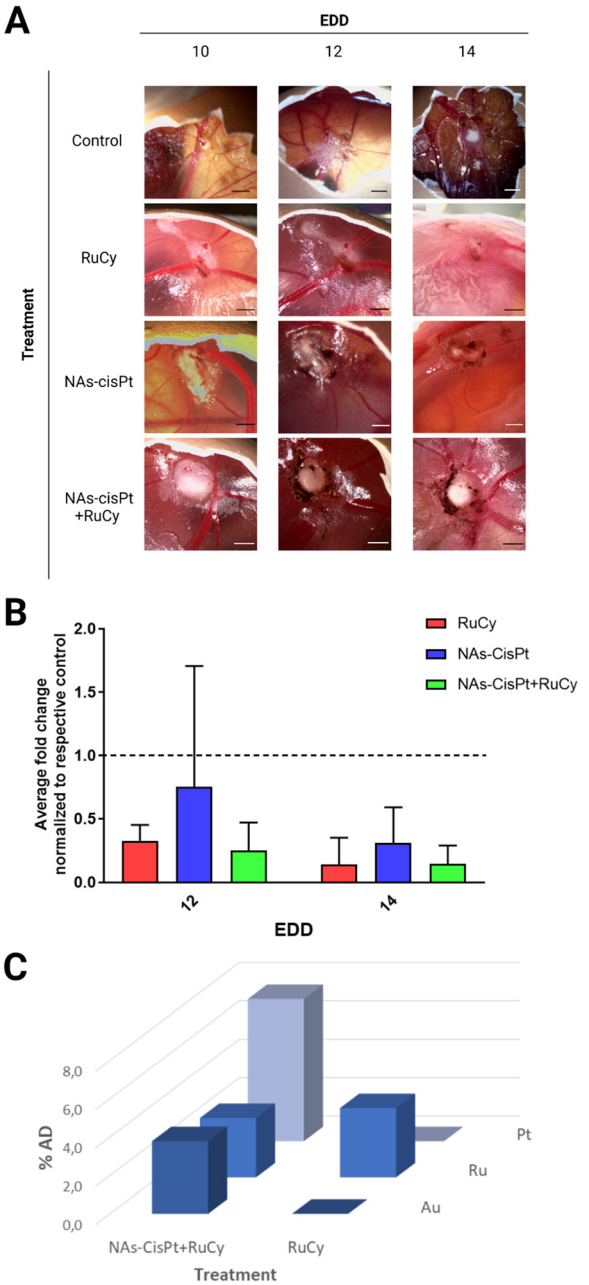

Fig. 3 Evaluation of the antitumor effect of RuCy and NAs-CisPt on CAM. (A) Representative images of tumor-bearing eggs on EDD10 (pre-treatment), EDD12 and EDD14. Scale bars: 2 mm. (B) Tumor volume fold change of each treatment condition calculated over control at each respective EDD. No statistical differences were noted among the treatment conditions. Statistical analysis was performed by two-way ANOVA (Tukey's multiple comparisons test). (C) ICP-MS quantification of ruthenium, gold and platinum in harvested tumors. The amounts of metals are reported as % administered dose (%AD) with at least 3 samples per condition.

for four days following the application of the treatment, and the volume was derived using a modified ellipsoid formula that considers the surface measurements of width and length (Fig. 3A).[31] Overall, medium-treated tumors showed an increased tumor volume fold change both at EDD12 and 14 compared to the pretreatment tumor size at EDD10. In contrast, a progressive

reduction of tumor fold change was observed for each treatment group between EDD10 and 14, suggesting that RuCy and NAs-CisPt remarkably inhibit tumor growth in both single and combined administration (Fig. S7, ESI†). The comparison of the treatment conditions with each specific EDD to the control denotes an improved size-reducing effect for both RuCy and NAs-CisPt + RuCy treated tumors compared to NAs-CisPt alone (Fig. 3B) but without a clear additive effect and no significant differences. The harvested tumors have been processed for the quantification of ruthenium, gold, and platinum content through ICP-MS analysis, which confirmed the accumulation of the metals in the tumors (Fig. 3C and Table S4, ESI†). The results demonstrated a comparable accumulation of ruthenium in tumors treated with RuCy and co-treated with NAs-CisPt + RuCy (3.6% and 3.1%, respectively), confirming that the presence of NAs-CisPt does not affect the RuCy accumulation in cells. As expected, the biodistribution profile of ruthenium in the embryo's organs was negligible, with %AD values lower than 0.05% (Fig. S8, ESI†). Comparable results were obtained for gold and platinum in a previous study.[21] Moreover, the embryo viability was not significantly affected after the application of increasing doses of RuCy (25, 50 and 100 μg) (Fig. S9, ESI†). Taken together, these findings suggest the biosafety of RuCy for *in vivo* application. Further biological investigations are needed to reach a proper synergistic effect between RuCy and NAs-CisPt on the regulation of the major cancer-promoting mechanisms.

4. Conclusions

An emerging ruthenium complex (RuCy) has been successfully (co)loaded inside NAs demonstrating that multiple chemotherapeutics can be inserted into the nano-architectures. A supra-additive action has been observed in both 2D and 3D models by the combination of NAs-CisPt with free RuCy. This finding is of particular interest as the reduction of the dose of cisplatin administered to patients can significantly reduce the associated side effects, resulting in a better prognosis. The evaluations in CAMs confirmed the promising antitumor activity of RuCy on developing organisms and evidenced its biosafety and the lack of ruthenium bioaccumulation in major organs, while an *in vitro* supra-additive effect was not corroborated. Our data confirm that the employment of alternative *in vivo* models is pivotal in oncological preclinical research to validate the *in vitro* findings within the 3Rs concept, unveil the molecular mechanism involved in cancer treatment response, and finally promote the advancement of innovative approaches to the clinic. The exploitation of gold USNPs in NAs may result in the potential employment of multi-drug-loaded NAs in combination with photothermal- or radio-therapy for integrated cancer management.[38,39] Overall, this work leads to the development of the next strategies for the treatment of oral malignancies based on nano-structured co-chemotherapeutics.

Notes

Data processed and graphs prepared by using GraphPad Prism software (version 8.0). The raw and processed data required to reproduce these findings are available on request to the Authors. The graphical abstract and Fig. 1 have been created with **https://BioRender.com**

Author contributions

M. S., V. F., cellular experiments and data analysis; V. F., M. L. E., A. K. M., A. Z., nano-architectures synthesis and characterizations, and ICP-MS quantification; P. S., A. G., N. G., V. F., A. K. M., A. Z., *in vivo* experiments and data analysis; L. B., synthesis and characterizations of the metal complexes; F. M. coordination of the metal complexes synthesis and characterizations; V. V., design and coordination of the project. All Authors have discussed the data and contributed to write the manuscript.

Conflicts of interest

The Authors declare no competing financial interests that could have appeared to influence the work reported in this paper.

Acknowledgements

The research leading to these results has received funding from AIRC under MFAG 2017-ID 19852 project-P. I. Voliani Valerio.

References

1 P. Bose, N. T. Brockton and J. C. Dort, Head and neck cancer: From anatomy to biology, *Int. J. Cancer*, 2013, **133**, 2013–2023, DOI: **10.1002/ijc.28112**.
2 F. dos, S. Menezes, G. A. Fernandes, J. L. F. Antunes, L. L. Villa and T. N. Toporcov, Global incidence trends in head and neck cancer for HPV-related and -unrelated subsites: A systematic review of population-based studies, *Oral Oncol.*, 2021, **115**, 105177, DOI: **10.1016/J.ORALONCOLOGY.2020.105177**.
3 H. Sung, J. Ferlay, R. L. Siegel, M. Laversanne, I. Soerjomataram, A. Jemal and F. Bray, Global Cancer Statistics 2020: GLOBOCAN Estimates of Incidence and Mortality Worldwide for 36 Cancers in 185 Countries, *Ca-Cancer J. Clin.*, 2021, **71**, 209–249, DOI: **10.3322/CAAC.21660**.
4 D. E. Johnson, B. Burtness, C. R. Leemans, V. W. Y. Lui, J. E. Bauman and J. R. Grandis, Head and neck squamous cell carcinoma, *Nat. Rev. Dis. Prim.*, 2020, **61**, 1–22, DOI: **10.1038/s41572-020-00224-3**.
5 J. D. Cramer, B. Burtness, Q. T. Le and R. L. Ferris, The changing therapeutic landscape of head and neck cancer, *Nat. Rev. Clin. Oncol.*, 2019, **16**, 669–683, DOI: **10.1038/s41571-019-0227-z**.
6 L. Q. M. Chow, Head and Neck Cancer, *N. Engl. J. Med.*, 2020, **382**, 60–72, DOI: **10.1056/NEJMra1715715**.
7 J. Gao, Z. Wang, J. Fu, A. Jiayu, Y. Ohno and C. Xu, Combination treatment with cisplatin, paclitaxel and olaparib has synergistic and dose reduction potential in ovarian cancer cells, *Exp. Ther. Med.*, 2021, **22**, 1–9, DOI: **10.3892/ETM.2021.10367**.
8 S. M. Meier-Menches, C. Gerner, W. Berger, C. G. Hartinger and B. K. Keppler, Structure–activity relationships for

ruthenium and osmium anticancer agents – towards clinical development, *Chem. Soc. Rev.*, 2018, **47**, 909–928, DOI: 10.1039/C7CS00332C.

9 S. Y. Lee, C. Y. Kim and T. G. Nam, Ruthenium complexes as anticancer agents: A brief history and perspectives, *Drug Des. Devel. Ther.*, 2020, **14**, 5375–5392, DOI: 10.2147/DDDT.S275007.

10 C. Riccardi, D. Musumeci, M. Trifuoggi, C. Irace, L. Paduano and D. Montesarchio, Anticancer ruthenium(III) complexes and Ru(III)-containing nanoformulations: An update on the mechanism of action and biological activity, *Pharmaceuticals*, 2019, **12**(4), 146, DOI: 10.3390/ph12040146.

11 E. Alessio and L. Messori, NAMI-A and KP1019/1339, Two Iconic Ruthenium Anticancer Drug Candidates Face-to-Face: A Case Story in Medicinal Inorganic Chemistry, *Mol.*, 2019, **24**, 1995, DOI: 10.3390/MOLECULES24101995.

12 B. S. Murray, M. V. Babak, C. G. Hartinger and P. J. Dyson, The development of RAPTA compounds for the treatment of tumors, *Coord. Chem. Rev.*, 2016, **306**, 86–114, DOI: 10.1016/j.ccr.2015.06.014.

13 A. Weiss, R. H. Berndsen, M. Dubois, C. Müller, R. Schibli, A. W. Griffioen, P. J. Dyson and P. Nowak-Sliwinska, In vivo anti-tumor activity of the organometallic ruthenium(ii)-arene complex [Ru(η6-p-cymene)Cl2(pta)] (RAPTA-C) in human ovarian and colorectal carcinomas, *Chem. Sci.*, 2014, **5**, 4742–4748, DOI: 10.1039/c4sc01255k.

14 M. Rausch, P. J. Dyson and P. Nowak-Sliwinska, Recent Considerations in the Application of RAPTA-C for Cancer Treatment and Perspectives for Its Combination with Immunotherapies, *Adv. Ther.*, 2019, **2**, 1900042, DOI: 10.1002/adtp.201900042.

15 M. Santi, A. K. Mapanao, L. Biancalana, F. Marchetti and V. Voliani, Ruthenium arene complexes in the treatment of 3D models of head and neck squamous cell carcinomas, *Eur. J. Med. Chem.*, 2021, **212**, 113143, DOI: 10.1016/j.ejmech.2020.113143.

16 E. Zanda, N. Busto, L. Biancalana, S. Zacchini, T. Biver, B. Garcia and F. Marchetti, Anticancer and antibacterial potential of robust Ruthenium(II) arene complexes regulated by choice of α-diimine and halide ligands, *Chem. – Biol. Interact.*, 2021, **344**, 109522, DOI: 10.1016/j.cbi.2021.109522.

17 L. Biancalana, L. K. Batchelor, T. Funaioli, S. Zacchini, M. Bortoluzzi, G. Pampaloni, P. J. Dyson and F. Marchetti, α-Diimines as Versatile, Derivatizable Ligands in Ruthenium(II) p-Cymene Anticancer Complexes, *Inorg. Chem.*, 2018, **57**, 6669–6685, DOI: 10.1021/acs.inorgchem.8b00882.

18 N. Joksimović, N. Janković, J. Petronijević, D. Baskić, S. Popovic, D. Todorović, M. Zarić, O. Klisurić, M. Vraneš, A. Tot and Z. Bugarčić, Synthesis, Anticancer Evaluation and Synergistic Effects with cis platin of Novel Palladium Complexes: DNA, BSA Interactions and Molecular Docking Study, *Med. Chem. (Los. Angeles)*, 2019, **16**, 78–92, DOI: 10.2174/1573406415666190128095732.

19 A. K. Mapanao, P. Sarogni, M. Santi, M. Menicagli, A. Gonnelli, A. Zamborlin, M. A. Ermini and V. Voliani, Pro-apoptotic and size-reducing effects of protein corona-modulating nanoarchitectures enclosing platinum prodrug in in vivo oral carcinoma, *Biomater. Sci.*, 2022, **10**, 6135–6145, DOI: 10.1039/D2BM00994C.

20 A. K. Mapanao, M. Santi, P. Faraci, V. Cappello, D. Cassano and V. Voliani, Endogenously Triggerable Ultrasmall-in-Nano Architectures: Targeting Assessment on 3D Pancreatic Carcinoma Spheroids, *ACS Omega*, 2018, **3**, 11796–11801, DOI: 10.1021/acsomega.8b01719.

21 P. Sarogni, A. K. Mapanao, A. Gonnelli, M. L. Ermini, S. Marchetti, C. Kusmic, F. Paiar and V. Voliani, Chorioallantoic membrane tumor models highlight the effects of cisplatin compounds in oral carcinoma treatment, *IScience*, 2022, **25**, 103980, DOI: 10.1016/j.isci.2022.103980.

22 A. K. Mapanao, G. Giannone, M. Summa, M. L. Ermini, A. Zamborlin, M. Santi, D. Cassano, R. Bertorelli and V. Voliani, Biokinetics and clearance of inhaled gold ultrasmall-in-nano architectures, *Nanoscale Adv.*, 2020, **2**(9), 3815–3820, DOI: 10.1039/d0na00521e.

23 A. Zamborlin, M. L. Ermini, M. Summa, G. Giannone, V. Frusca, A. K. Mapanao, D. Debellis, R. Bertorelli and V. Voliani, The Fate of Intranasally Instilled Silver Nanoarchitectures, *Nano Lett.*, 2022, **22**(13), 5269–5276, DOI: 10.1021/acs.nanolett.2c01180.

24 C. Avigo, D. Cassano, C. Kusmic, V. Voliani and L. Menichetti, Enhanced Photoacoustic Signal of Passion Fruit-Like Nanoarchitectures in a Biological Environment, *J. Phys. Chem. C.*, 2017, **121**, 6955–6961, DOI: 10.1021/acs.jpcc.6b11799.

25 D. Cassano, M. Santi, F. D'Autilia, A. K. Mapanao, S. Luin and V. Voliani, Photothermal effect by NIR-responsive excretable ultrasmall-in-nano architectures, *Mater. Horizons.*, 2019, **6**, 531–537, DOI: 10.1039/C9MH00096H.

26 A. K. Mapanao, P. P. Che, P. Sarogni, P. Sminia, E. Giovannetti and V. Voliani, Tumor grafted – chick chorioallantoic membrane as an alternative model for biological cancer research and conventional/nanomaterial-based theranostics evaluation, *Expert Opin. Drug Metab. Toxicol.*, 2021, **17**, 947–968, DOI: 10.1080/17425255.2021.1879047.

27 P. Sarogni, A. K. Mapanao, S. Marchetti, C. Kusmic and V. Voliani, A Standard Protocol for the Production and Bioevaluation of Ethical In Vivo Models of HPV-Negative Head and Neck Squamous Cell Carcinoma, *ACS Pharmacol. Transl. Sci.*, 2021, **4**, 1227–1234, DOI: 10.1021/acsptsci.1c00083.

28 M. D. Hall, C. T. Dillon, M. Zhang, P. Beale, Z. Cai, B. Lai, A. P. J. Stampfl and T. W. Hambley, The cellular distribution and oxidation state of platinum(II) and platinum(IV) antitumour complexes in cancer cells, *J. Biol. Inorg. Chem.*, 2003, **8**, 726–732, DOI: 10.1007/s00775-003-0471-6.

29 S. Dhar, W. L. Daniel, D. A. Giljohann, C. A. Mirkin and S. J. Lippard, Polyvalent oligonucleotide gold nanoparticle conjugates as delivery vehicles for platinum(IV) warheads, *J. Am. Chem. Soc.*, 2009, **131**, 14652–14653, DOI: 10.1021/ja9071282.

30 M. Santi, A. K. Mapanao, V. Cappello and V. Voliani, Production of 3D Tumor Models of Head and Neck Squamous Cell Carcinomas for Nanotheranostics Assessment, *ACS Biomater. Sci. Eng.*, 2020, **6**, 4862–4869, DOI: 10.1021/acsbiomaterials.0c00617.

31 M. Rovithi, A. Avan, N. Funel, L. G. Leon, V. E. Gomez, T. Wurdinger, A. W. Griffioen, H. M. W. Verheul and E. Giovannetti, Development of bioluminescent chick chorioallantoic membrane (CAM) models for primary pancreatic cancer cells: A platform for drug testing, *Sci. Rep.*, 2017, **7**, 1–13, DOI: **10.1038/srep44686**.

32 M. Santi, A. K. Mapanao, D. Cassano, Y. Vlamidis, V. Cappello and V. Voliani, Endogenously-Activated Ultrasmall-in-Nano Therapeutics: Assessment on 3D Head and Neck Squamous Cell Carcinomas, *Cancers (Basel)*, 2020, **12**, 1063, DOI: **10.3390/cancers12051063**.

33 A. J. Trinidad, S. J. Hong, Q. Peng, S. J. Madsen and H. Hirschberg, Combined concurrent photodynamic and gold nanoshell loaded macrophage-mediated photothermal therapies: An in vitro study on squamous cell head and neck carcinoma, *Lasers Surg. Med.*, 2014, **46**, 310–318, DOI: **10.1002/LSM.22235**.

34 K. Cho, X. Wang, S. Nie, Z. (Georgia) Chen and D. M. Shin, Therapeutic Nanoparticles for Drug Delivery in Cancer, *Clin. Cancer Res.*, 2008, **14**, 1310–1316, DOI: **10.1158/1078-0432.CCR-07-1441**.

35 A. K. Mapanao and V. Voliani, Three-dimensional tumor models: Promoting breakthroughs in nanotheranostics translational research, *Appl. Mater. Today.*, 2020, **19**, 100552, DOI: **10.1016/j.apmt.2019.100552**.

36 M. A. G. Barbosa, C. P. R. Xavier, R. F. Pereira, V. Petrikaitė and M. H. Vasconcelos, 3D Cell Culture Models as Recapitulators of the Tumor Microenvironment for the Screening of Anti-Cancer Drugs, *Cancers*, 2021, **14**, 190, DOI: **10.3390/CANCERS14010190**.

37 T. Rodrigues, B. Kundu, J. Silva-Correia, S. C. Kundu, J. M. Oliveira, R. L. Reis and V. M. Correlo, Emerging tumor spheroids technologies for 3D in vitro cancer modeling, *Pharmacol. Ther.*, 2018, **184**, 201–211, DOI: **10.1016/J.PHARMTHERA.2017.10.018**.

38 P. P. Che, A. K. Mapanao, A. Gregori, M. L. Ermini, A. Zamborlin, M. Capula, D. Ngadimin, B. J. Slotman, V. Voliani, P. Sminia and E. Giovannetti, Biodegradable Ultrasmall-in-Nano Architectures Loaded with Cisplatin Prodrug in Combination with Ionizing Radiation Induces DNA Damage and Apoptosis in Pancreatic Ductal Adenocarcinoma, *Cancers (Basel)*, 2022, **14**, 3034, DOI: **10.3390/cancers14123034**.

39 A. K. Mapanao, M. Santi and V. Voliani, Combined chemo-photothermal treatment of three-dimensional head and neck squamous cell carcinomas by gold nano-architectures, *J. Colloid Interface Sci.*, 2021, **582**, 1003–1011, DOI: **10.1016/j.jcis.2020.08.059**.

